

On Prism Cross-Dispersers - Modelling Échelle Spectrograms

Jakob Wierzbowski*

Walter Schottky Institut der TU München, Am Coulombwall 4, 85748 Garching bei München

Bernd Bitnar[†] and Siegfried Hold[†]

In this paper, we elaborate on correctly predicting Échelle spectrograms by employing the fully three-dimensional representation of Snell's law to model the effects of prisms as cross-dispersers in Échelle spectrographs. We find that it is not sufficient to simply apply the frequently used trigonometric prism dispersion equation to describe recorded spectra. This vector equation approach is not limited to a single dispersive element when modelling multi-prism cross-disperser configurations. Our results help to understand the main levers in an Échelle spectrograph as well as contribute to auto-calibration algorithms for minimizing calibration efforts in daily operation.

Keywords: Prism; Echelle; Cross-Disperser; Snell's law; Sellmeier; QtYETI

INTRODUCTION

PRISMS are key parts in compact Échelle spectrographs which, in turn, are widely used in astrospectroscopy [1–4]. The advantage of prisms as dispersive elements is their high optical efficiency and transmittance in contrast to optical gratings. Unlike gratings, prisms do not diffract incident light into multiple orders but rather refract it into specific directions. To harvest the largest amount of light while covering a large spectral band, a common approach is to first disperse collimated light on a blazed, reflective optical grating with a low groove density on the order of $d = 30$ to 80 mm^{-1} and subsequently cross-disperse the diffracted light via a prism before focusing it down onto a detector using a lens. The low groove density helps to generate multiple overlapping orders ($m = 20$ to 60), e.g. in the visible range. At the same time, Échelle gratings are specifically designed with comparably high blaze angles ($\theta_B > 60^\circ$). Using them close to the Littrow condition $\alpha \approx \beta$ for highest optical efficiency, Échelle grating typically exhibit a large geometrical width. This increases the number of illuminated grooves. Both design parameters in turn help to achieve a high resolution $R = \lambda/\Delta\lambda$. An elaborate discussion on grating physics and blazed gratings is beyond the scope of this work. Comprehensive and beginner-friendly books on grating physics and astrospectroscopy with Écheltes can be found in [5] and [6], respectively.

Nevertheless, the dispersion relation of a diffraction grating is accurately described by the heuristic equation:

$$m \cdot \lambda = d(\sin \alpha + \sin \beta) \cos \gamma, \quad (1)$$

where m is the order number, λ the wavelength, d the grating constant, α and β the in- and outgoing angles, respectively. γ is the relative angle with respect to the plane of incidence, thus, perpendicular to α and β .

Employing equation (1), we use the standard convention of measuring angles *from* the grating normal **GN** *towards* the in- and outgoing beam, respectively [5]. Angles that are measured in clockwise/counter-clockwise di-

rection are negative/positive. Figure 1a summarizes this convention. Here, the incident angle α and the outgoing angles β_b and β_r are negative since they are measured in clockwise direction *from* the grating normal **GN**. In stark contrast to gratings, which exploit interference at periodic structures to diffract light, prisms on the other hand disperse light by refraction driven by a wavelength dependent refractive index within media [7] such as glasses.

MODELLING ÉCHELLES

Geometric prism equation

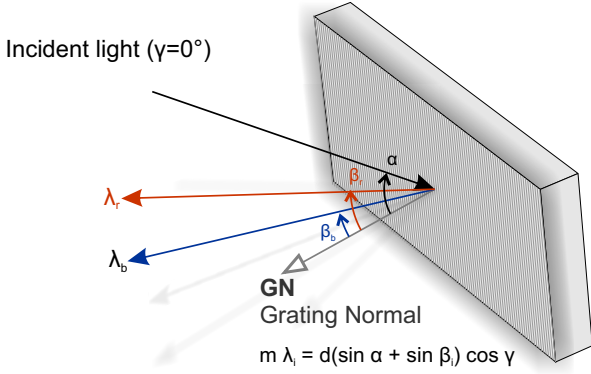
Figure 1b shows how incident light entering a prism at an angle θ_1 is refracted according to Snell's law $n_1 \cdot \sin \theta_1 = n_2 \cdot \sin \theta_2$, with n_1 and n_2 being the refractive indices of e.g. air and the prism medium (e.g. glass, $n > 1$), respectively. Both angles, θ_1 and θ_2 are measured relative to the surface normal describing the optical interface. The same principle applies to light exiting the prism. Using Snell's law, trigonometric relations as well as setting $n_1 = 1$, we can approximate the total refraction angle $\Phi(\lambda)$ to be:

$$\Phi(\lambda) = \arcsin [n_\lambda \cdot \sin \alpha - \arcsin(\sin \theta / n_\lambda)] + \theta - \alpha, \quad (2)$$

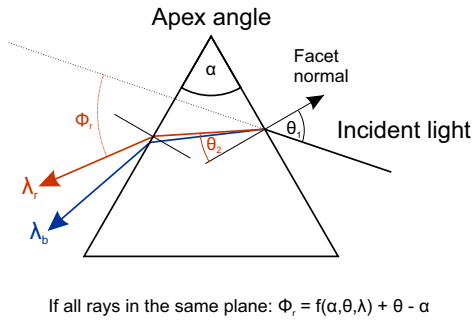
where α is the apex angle of the prism, $\theta = \theta_1$ is the angle between the prisms surface normal and the incoming beam as well as $n_\lambda = n_2$ being the wavelength dependent refractive index of the prism. For glass prisms, the refractive index is best described by the Sellmeier equation [8] (see supplementary material).

Please note, equation (2) is a strong simplification, which will turn out to deliver incorrect results when trying to predict Échelle spectra. It only applies when incoming and outgoing light lies in the same plane as the facet's surface normal vector.

a Grating



b Prism



c Cross Dispersion

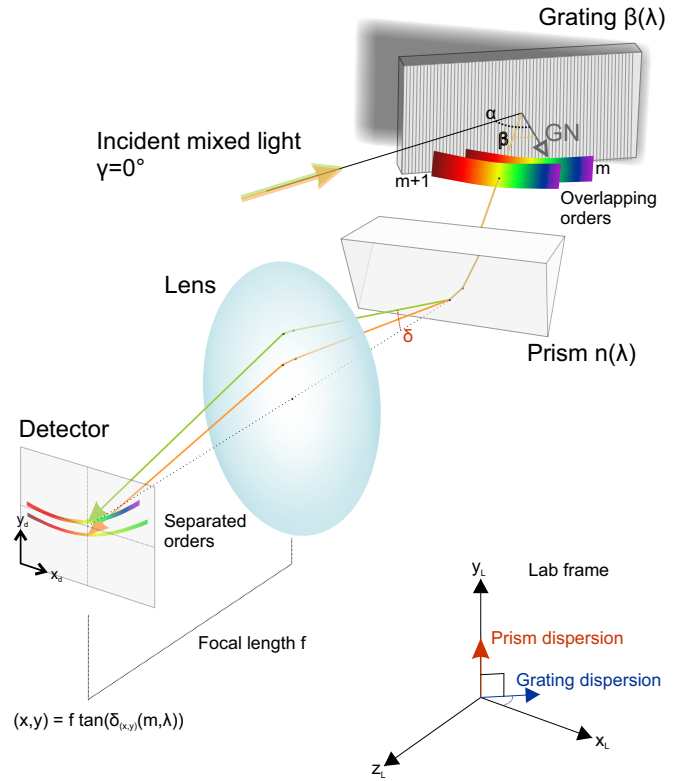


FIG. 1. Principles of dispersion. **a.** Diffraction Grating **b.** Dispersion prism. **c.** Cross-Disperser principle. Light incident on a grating at angles (α, γ) is diffracted into the direction β according to the grating equation. The resulting and overlapping orders m_i travel through a prism whose dispersion direction is perpendicular relative to the grating (red and blue arrows). This principle separates overlapping spectral orders into unique positions on the detector.

Cross-dispersion with prisms

Échelle spectrographs often use diffraction gratings with a low number of grooves per mm as main dispersing element in combination with, either, a second grating oriented perpendicularly to the first one, or a *prism*. Due to the low groove density, the diffraction orders tend to strongly overlap for $|m| > 20$ in the visible range [5, 6]. Therefore, disentangling the light for different orders becomes a necessity. Figure 1c shows a typical Échelle cross-disperser configuration, where the second dispersion element is a prism. A collimated beam of light that is parallel to the laboratory xz -plane ($\gamma = 0^\circ$) hits the surface of a reflective diffraction grating at a fixed angle α . The grating disperses the light in the xz -plane into multiple and most importantly overlapping orders m_i . Here, α and the outgoing angle β are negative with respect to the grating normal **GN**. Taking a step back to the grating equation (1), it is worth noting that the left side of the equation is changing, both, with λ and m . For a fixed observation angle $\beta = \text{const.}$, the right-hand side of the equation becomes a set of constants.

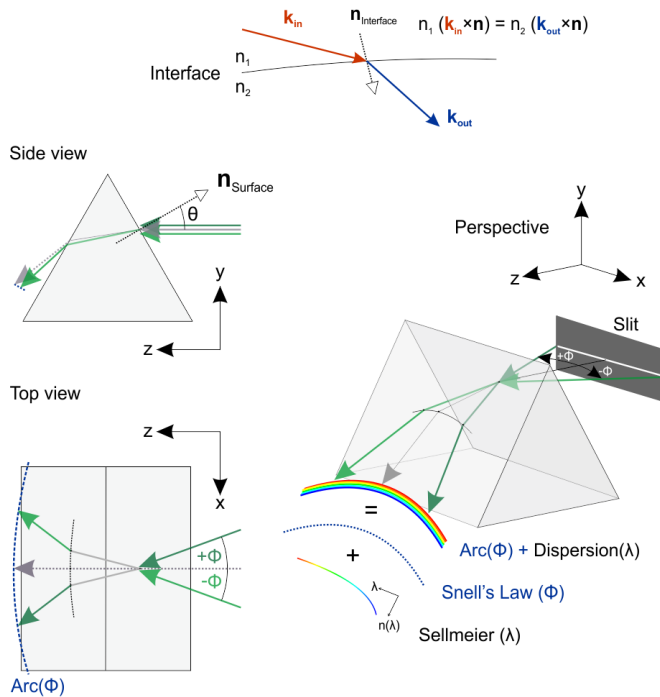
Suppose $\beta = \beta_o = \beta_g = \text{const.}$, it is then possible to

find two wavelengths λ_o and λ_g , such that:

$$m_o \lambda_o = m_g \lambda_g, \quad m_{o,g} \in \mathbb{Z} \setminus \{0\} \quad (3)$$

Thus, equation (3) dictates that two wavelengths from different orders satisfying this relation will be diffracted into the same direction. The two arrows (orange and green) in Figure 1c represent two beams of light with wavelengths λ_o and λ_g , respectively. Both beams are diffracted into the same direction depicted by the angle β whilst belonging to neighbouring diffraction orders m_o and $m_g = m_o + 1$. Upon exiting the prism at the second facet, both light rays will leave the prism under different angles, as previously explained in Figure 1b. Subsequently, an objective lens focuses these light beams onto a detector. The position y_d on the detector is determined by the angle δ of the green/orange light beam relative to the optical axis of the lens and its focal length f , thus, $y_d = f \cdot \tan \delta$. Since $\delta_o \neq \delta_g$, both light rays will be focused onto different points $(x_d, y_{d,o})$ and $(x_d, y_{d,g})$ on the detector. Applying this principle to all available light beams within the field of view of the prism and lens, we are now able to separate all physical orders.

a 3D Snell's Law



b

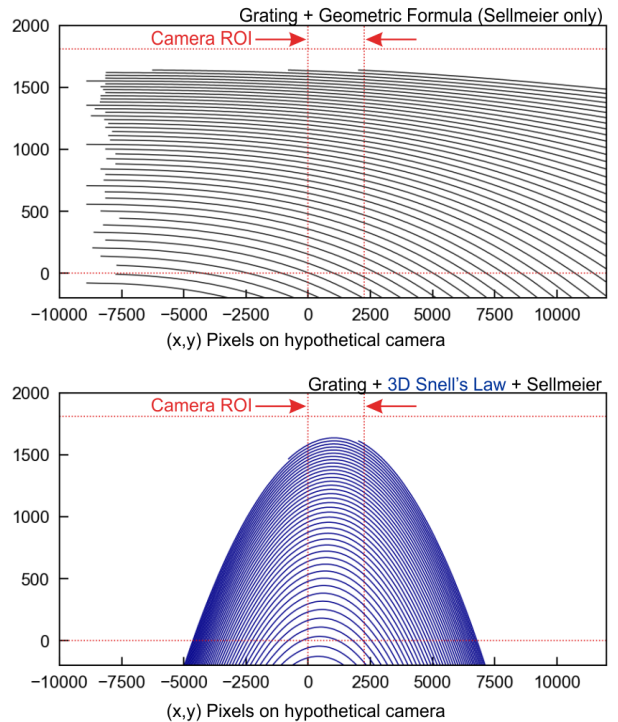


FIG. 2. Snell's Law in three dimensions. **a. Upper panel:** Vector-form of Snell's law describing the refraction of light beams traversing the interface between two media n_1 and n_2 . **Lower panel:** Dispersion of white light in prisms. Light from a line-source entering a prism will be dispersed and warped into a bow due to geometrical effects. **b.** Simulated cross-dispersed Échelle spectrograms using the geometric dispersion equation for prisms (upper panel) and simulated spectra using the three-dimensional equation for Snell's law (lower panel).

Snell's law in vector form

In the previous example, we considered the prism's entry facet normal vector to be in the same plane as the in- and outgoing light. In general, this assumption is not applicable and the geometric prism equation (2) breaks down. How do we want to tackle this issue?

Our approach is applying Snell's law in three dimensions

to the entry and exit facets of the prism using:

$$n_1 (\mathbf{k}_{in} \times \mathbf{n}) = n_2 (\mathbf{k}_{out} \times \mathbf{n}), \quad (4)$$

where n_1, n_2 are the refractive indices of two adjacent media, $\mathbf{k}_{in}, \mathbf{k}_{out}$ are the normalized incoming and outgoing beam direction vectors while \mathbf{n} is the normal vector of the entry surface. Using vector algebra identities, \mathbf{k}_{out} can be represented as a function of \mathbf{n} and \mathbf{k}_{in} (see supplementary material section):

$$\mathbf{k}_{out}(\mathbf{n}, \mathbf{k}_{in}) = \left(\sqrt{1 - \left(\frac{n_1}{n_2}\right)^2 [1 - (\mathbf{n} \cdot \mathbf{k}_{in})^2]} - \frac{n_1}{n_2} (\mathbf{n} \cdot \mathbf{k}_{in}) \right) \cdot \mathbf{n} + \frac{n_1}{n_2} \mathbf{k}_{in} \quad (5)$$

This equation does not contain tedious trigonometric functions but rather consists of scalar products that can be computed fairly fast [9, 10] which is why most ray tracing applications [11, 12] rely on this formula as it turned out during our literature research.

We summarised our findings in Figure 2. The upper panel in **a** depicts a light beam crossing an interface.

The incoming ray \mathbf{k}_{in} (red arrow) traverses the interface between two media with refractive indices n_1 and n_2 with $n_2 > n_1$, respectively. It is refracted towards the surface normal vector \mathbf{n} according to Snell's law. The resulting light ray is represented by the blue arrow \mathbf{k}_{out} . Without loss of generality, we apply this equation to an equilateral prism as shown in the lower panel of Figure 2a.

Here, we choose a point on the prism and model a small horizontal slit by two beams. These beams emerge from the edges of the slit at angles $\pm\phi$ relative to the z-axis and an entry point on the prism. Equation (5) dictates that the incoming beams will be refracted onto an arc (dashed black inner arc, see supplementary information). This indeed also applies when both beams leave the prism (blue dashed arc). Since different colours are dispersed into slightly different angles, the resulting arc will be dispersed along the z- and negative y-direction in our laboratory frame as a result of a wavelength dependent refractive index (Sellmeier equation). This behaviour cannot be completely modelled via the frequently used trigonometric equation (2). To visually understand this better, we prepared an interactive online example using the tool on *Math3D.org* [13]. A Python implementation and a simple calculation can be found in the appendix.

Dispersing and warping the incident light into an arc, the prism has a strong effect on spectrograms taken with Échelle spectrometers in a Grating-Prism configuration. Figure 2b contrasts computed spectra using the trigonometric prism equation (2) and the vectorial equation (5). The upper panel is a simulated cross-dispersed spectrogram (black) which was obtained using the geometrical equation (2) whilst the lower panel depicts a spectrogram simulated with the vectorial approach (blue). We compressed the x-direction of the detector to visualise the differences also outside of a typical camera region of interest (ROI). In the upper panel of Figure 2b, we can clearly see all spectral orders having a monotonically decreasing behaviour for ever larger x-values. In our calculations, shorter wavelengths of a respective order appear at larger x-pixel values. We can observe the direct influence of the Sellmeier equation on the dispersion behaviour, since equation (2) only accounts for θ , the entry angle in the yz-plane, and the wavelength dependent refractive index.

The spectrogram strongly changes in the second case as Snell's Law in its vector form accounts for both, θ and ϕ . The latter being the entry angle in the xz-plane (see Fig. 2a, lower left panel). This method correctly describes and predicts the shape and positions of spectral orders on a detector. Please note, that the calculated spectra depend on geometrical parameters such as grating position, prism angles, detector rotation, etc. Thus, fitting spectra or single wavelengths in a measured spectrum enables the determination of the actual angles and positions of the optical components.

ThAr cold-cathode-lamps with distinct single peaks are a great candidate for this. These lamps are typically used to calibrate Échelle spectrograms [6] and are within the standard toolset of professional and enthusiast astronomers. Our approach has the potential to save time during calibration and enables algorithms for auto-calibrations or tracing thermal drifts in longer measurement campaigns.

COMPARISON AND OUTLOOK

In Figure 3a, we compare our findings using the vectorial representation of Snell's law with real Échelle spectra taken with a FLECHAS spectrograph, designed by Carlos Guirao and colleagues [14][15]. In our case, the spectrometer is equipped with a $d = 79$ lines/mm grating, a 60 mm Schott glass N-F2 prism, an $f = 200$ mm objective lens as well as a 4524×3624 pixel camera with a pixel size of $6 \mu\text{m}$. The spectra and calculations were carried out using a full 2×2 pixel binning. To perform the calculations properly, we extracted the spectrometer geometry from available CAD files [14]. For contrast reasons, we plotted a measured spectrogram of a table-top tungsten lamp (flat field spectrum) in light blue and overlaid a calculated spectrogram with dashed black lines using the vectorial approach. The red dots in the image correspond to measured ThAr peaks on the same spectrometer. At the same time, the green boxes mark simulated spectral positions for selected Ar and Th catalogue lines from NIST [16]. Here, the calculated orders range from $|m| = 19$ to 57. The overlap between these spectrograms is very good due to proper spectrometer alignment and slightly adjusted simulation parameters (detector rotation, magnification, etc.) based on the spectrometer geometry. An enlarged version of Figure 3a can be found in the supplementary information (Figure 9).

We will make our simulation package QtYETI [17] available on github which includes the vectorial approach.

This satisfying result of course leads to the question, if the algorithm is applicable to cross-dispersers with a serial arrangement of dispersion prisms. Figure 3b shows two possible scenarios. The left sketch shows a single prism configuration that can be found in FLECHAS and other Échelle spectrometers. Light that has been dispersed in the xz-plane by a grating hits the prism facet and is then further dispersed in the yz-plane and eventually focused on a detector. The resulting spectrogram is shown in Figure 3c (upper panel). Within an arbitrary, yet, fixed interval (red arrow) we find 29 orders. The spectrogram changes significantly, if we now introduce another prism (Fig. 3b, lower right panel, N-F2 glass) and change the camera angle such that the beginning of the 20th order starts at the same pixel (see supplementary information). Within the same fixed interval as before, we clearly see a wider dispersion resulting in only 18 orders. This is of course to be expected as another prism further disperses the incoming light in the yz-plane. This double prism configuration can be found in white-pupil spectrometers to further fold the beam path while increasing dispersion. Further details can be found in [18].

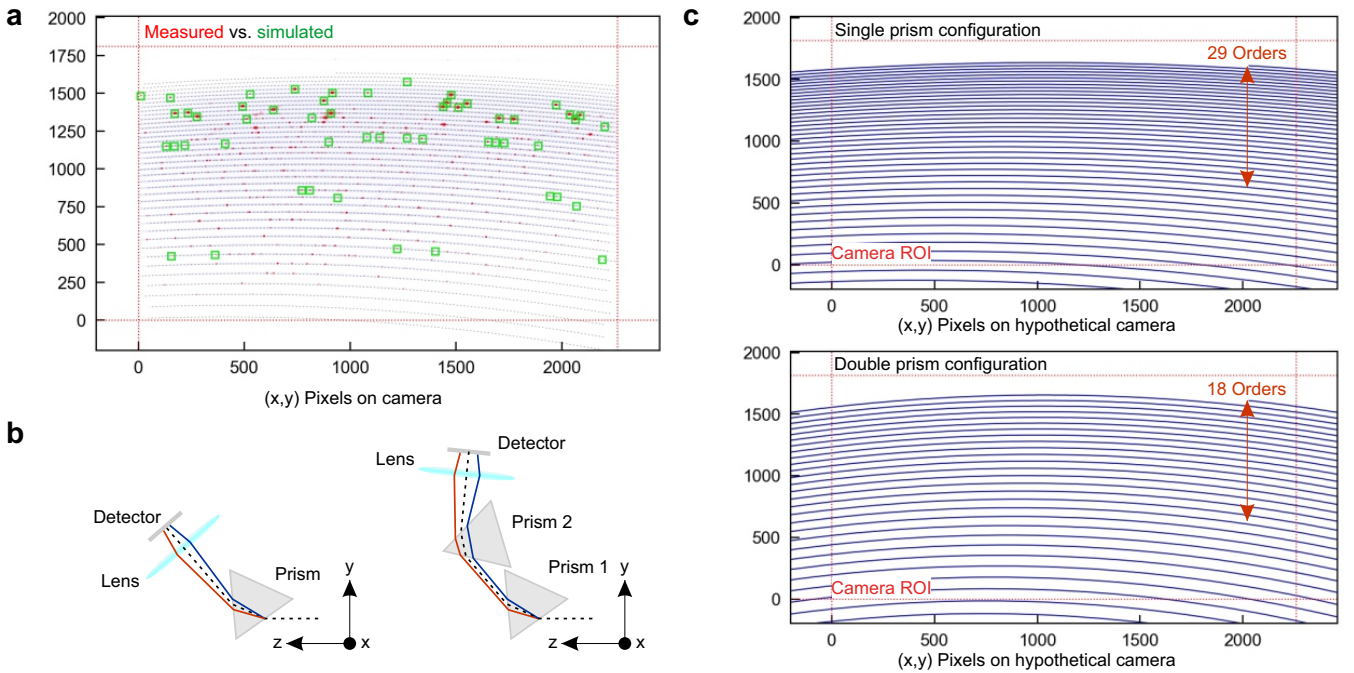


FIG. 3. Comparison of simulation and measurement. **a**. Overlay of a measured flat field spectrum of a tungsten lamp on a FLECHAS spectrometer (light blue) and a simulated Échelle spectrum (black, dashed lines). The red dots are measured ThAr peaks. The green boxes are simulated ThAr peak positions for selected Argon and Thorium lines from *nist.gov*. The overlap is very good over all visible orders. This good agreement is achieved through proper consideration of the spectrometer geometry in the simulation. **b**. Single prism and double prism cross-disperser arrangement. The double-prism configuration is used e.g. in white pupil spectrometers to achieve good separation of the orders and folding the beam path. **c**. Simulation of a spectrogram with a single prism cross-disperser (upper panel) and double-prism configuration (lower panel). The red arrow of constant length helps to show how the second prism introduces more dispersion and a stronger bending behaviour of the spectral orders towards lower x pixel values.

SUMMARY

In this work, we have shown how two-dimensional Échelle spectrograms emerge from using a grating-prism cross-dispersion configuration. We used Snell's law in its vector form as a basis for our calculations and correctly predicted the shape and position of grating diffraction orders for grating-prism Échelle spectrographs. We have found significant differences between using the common trigonometric prism dispersion equation and a full vectorial representation of Snell's law. We continued to show a quantitatively good overlap between calculated and measured spectra for a FLECHAS spectrograph. In the last part, we applied our simulation code to a double-prism configuration with reasonable results, which could easily be verified in a laboratory setup.

In the next steps we will continue our work to accomplish a robust way to auto-calibrate a spectrometer and Échelle spectra using a ThAr-Lamp (thorium argon). Our algorithms will be implemented in the user-friendly cross-platform open-source data reduction software **QtYETI** written in Python.

The authors want to thank Lothar Schanne, Klaus Vollmann, Ulrich Waldschlaeger, Herbert Pühringer and

Daniel Sablowski for valuable inputs and discussions as well as corrections from Annette Fälschle, Lukas Hanschke & Friedrich Sbresny.

* jakob.wierzbowski@wsi.tum.de

† Contributed equally to this work

- [1] D. J. Schroeder and C. M. Anderson, *PASP* **83**, 438 (1971).
- [2] S. S. Vogt, *PASP* **99**, 1214 (1987).
- [3] I. Appenzeller, J. Krautter, H. Mandel, and R. Oestreich, in *ESA Special Publication*, ESA Special Publication, Vol. 2, edited by N. Longdon and E. J. Rolfe (1988) pp. 337–340.
- [4] K. G. Strassmeier, I. Ilyin, and M. Steffen, *AAP* **612**, A44 (2018), [arXiv:1712.06960 \[astro-ph.SR\]](https://arxiv.org/abs/1712.06960).
- [5] C. Palmer, *Diffraction Grating Handbook (7th edition)* (2014).
- [6] L. Schanne and D. Sablowski, *Astrophysikalische Instrumentierung und Messtechnik für die Spektroskopie: Theorie, Praxis, Technik und Beobachtung*, 1st ed. (Schanne, Lothar F, Mannheim, Germany, 2018).
- [7] D. J. Griffiths, *Introduction to Electrodynamics* (Pearson, 2013).

- [8] W. von Sellmeier, *Annalen der Physik* **219**, 272 (1871).
- [9] A. Miks and P. Novak, *JOSA A* **29**, 1356 (2012).
- [10] Frobenius and Stack Exchange, Snell's law in vector form, <https://physics.stackexchange.com/questions/435512/snells-law-in-vector-form> (2018), accessed: 2023-5-3.
- [11] T. Whitted, *Commun. ACM* **23**, 343–349 (1980).
- [12] A. S. Glassner, ed., *An introduction to ray tracing* (Morgan Kaufmann, Oxford, England, 1989).
- [13] J. Wierzbowski, Prism refraction via Snell's Law in 3D, <https://www.math3d.org/b4TzRiJ1M> (2022).
- [14] C. Guirao, Integrating FLECHAS, a breadboard Echelle spectrograph, <https://spectroscopy.wordpress.com/2010/05/14/integrating-an-optical-bench-echelle-spectrograph/> (2010).
- [15] M. Mugrauer, G. Avila, and C. Guirao, *Astronomische Nachrichten* **335**, 417.
- [16] NIST - National Institute of Standards and Technology, *Basic atomic spectroscopic data*. (2023).
- [17] J. Wierzbowski, *QtYETI - Yeti's Extra-Terrestrial Investigations* (2023).
- [18] D. P. Sablowski, M. Woche, M. Weber, A. Järvinen, and K. G. Strassmeier, in *Advances in Optical and Mechanical Technologies for Telescopes and Instrumentation III*, Vol. 10706, edited by R. Navarro and R. Geyl, International Society for Optics and Photonics (SPIE, 2018) p. 107066F.
- [19] Schott AG, *Refractive indices of prisms*. (2023).

SUPPLEMENTARY MATERIAL

Sellmeier's Equation

The Sellmeier equation describes the refractive index of glasses within visible wavelength range and slightly beyond [8].

$$n(\lambda) = \sqrt{1 + \sum_{i=1, \dots, n} \frac{B_i \lambda^2}{\lambda^2 - C_i}}$$

In this work, we used the below coefficients to successfully model our Échelle spectra which are taken from [19]

Coefficients	B_i	C_i
N-F2	B1 = 1.34533359	C1 = 0.00997743871
	B2 = 0.209073176	C2 = 0.0470450767
	B3 = 0.93757162	C3 = 111.8867640
N-NF2	B1 = 1.39757037	C1 = 0.00995906143
	B2 = 0.159201403	C2 = 0.0546931752
	B3 = 1.2686543	C3 = 119.248346

Grating equation

The derivation and complete discussion of the grating equation can be found in the MKS Grating Handbook which can be found on <https://www.newport.com>

$$m \cdot \lambda = d(\sin \alpha + \sin \beta) \cos \gamma$$

We use the following convention: every angle is measured from the grating normal GN towards any beam of light. If the rotation is clockwise or counter-clockwise, the corresponding angle is negative or positive, respectively. α is the angle of incidence relative to the grating normal. β is the outgoing angle of the diffracted light for an order m and m is the grating constant.

Example: A 79 grooves/ μm grating exhibits a grating constant $d = 1/79\text{mm} = 12 \mu\text{m}/\text{groove}$. The angle γ , which we treated as $\gamma = \text{deg } 0$ for simplicity, is the out-of-plane angle of light with respect to the plane of incidence of a grating (if the grating vector $G = (2\pi/d) \cdot \mathbf{g}$ lies perfectly parallel to the xz -plane). \mathbf{G} is the reciprocal grating vector. For constant observation angles, the right-hand side of grating equation $m \cdot \lambda = d(\sin \alpha + \sin \beta) \cos \gamma$ becomes constant and can be solved for multiple combinations of m and λ . Suppose $\alpha = -67^\circ$, $\beta = -58^\circ$, $\gamma = 0^\circ$, $d = 79 \text{ grooves}/\mu\text{m}$, then $m \cdot \lambda = -22.30 \mu\text{m}$. If $m = -20, -21, -22, \dots$ and $\lambda = 1.115 \mu\text{m}, 1.062 \mu\text{m}, 1.014 \mu\text{m}, \dots$

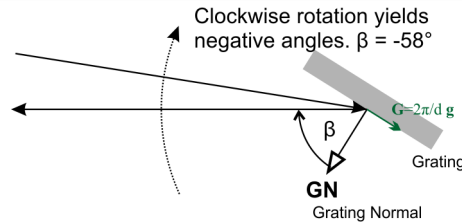


FIG. 4. Grating angle definition.

3D Snell's Law

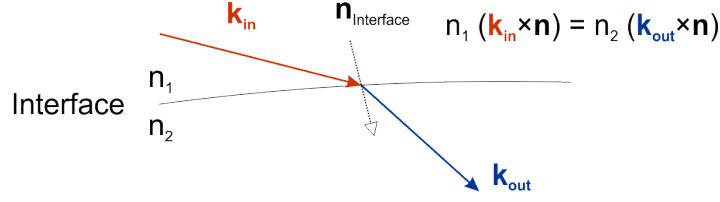


FIG. 5. General application of Snell's law.

Derivation of Snell's law into a scalar product equation

Snell's law can be expressed as:

$$n_1 (\mathbf{n} \times \mathbf{k}_{in}) = n_2 (\mathbf{n} \times \mathbf{k}_{out})$$

Please note, we will use the general definition $\mathbf{k} = \mathbf{k}^{ip} + \mathbf{k}^{op}$, where $\mathbf{k}^{ip} = \mathbf{k} - (\mathbf{n} \cdot \mathbf{k}) \mathbf{n}$ and $\mathbf{k}^{op} = (\mathbf{n} \cdot \mathbf{k}) \mathbf{n}$ are the in-plane and out-of-plane components of a generic vector \mathbf{k} with respect to a surface normal vector \mathbf{n} .

With the relation $\mathbf{a} \times \mathbf{b} = |\mathbf{a}| |\mathbf{b}| \sin \theta$, we obtain the known relation $n_1 \sin \theta_1 = n_2 \sin \theta_2$, as \mathbf{k} and \mathbf{n} are of unit length. By applying $(\mathbf{n} \times)$ to both sides of the upper equation and by means of the vector identity $\mathbf{A} \times (\mathbf{B} \times \mathbf{C}) = (\mathbf{A} \cdot \mathbf{C}) \mathbf{B} - (\mathbf{A} \cdot \mathbf{B}) \mathbf{C}$, we can transform Snell's law into:

$$-\frac{n_1}{n_2} [\mathbf{k}_{in} - (\mathbf{n} \cdot \mathbf{k}_{in}) \mathbf{n}] = \mathbf{k}_{out} - (\mathbf{n} \cdot \mathbf{k}_{out}) \mathbf{n} =: \mathbf{k}_{out}^{ip}$$

Both sides of the equation correspond to in-plane components of \mathbf{k}_{in} and \mathbf{k}_{out} , respectively. This results from $\mathbf{k}^{op} = (\mathbf{n} \cdot \mathbf{k}) \mathbf{n}$ being the out-of-plane component of a vector \mathbf{k} . We can now express the in-plane component of \mathbf{k}_{out}^{ip} in terms of \mathbf{k}_{in} and the refractive indices. The next step is calculating the out-of-plane component of \mathbf{k}_{out}^{op} as a function of \mathbf{k}_{in} .

The squared length of \mathbf{k}_{out} can be written as:

$$\begin{aligned} k_{out}^2 &= \mathbf{k}_{out}^{op} \cdot \mathbf{k}_{out}^{op} + \mathbf{k}_{out}^{ip} \cdot \mathbf{k}_{out}^{ip} \\ &= \mathbf{k}_{out}^{op} \cdot \mathbf{k}_{out}^{op} + \left(\frac{n_1}{n_2}\right)^2 [(\mathbf{n} \cdot \mathbf{k}_{in}) \mathbf{n} - \mathbf{k}_{in}] \cdot \left(\frac{n_1}{n_2}\right)^2 [(\mathbf{n} \cdot \mathbf{k}_{in}) \mathbf{n} - \mathbf{k}_{in}] \end{aligned}$$

with $\mathbf{k}^{ip} \cdot \mathbf{k}^{op} = 0$, since and thus both vectors are defined as orthogonal to one another.

After multiplicative expansion and subsequent simplification of the upper expression, we obtain:

$$k_{out}^2 = \mathbf{k}_{out}^{op} \cdot \mathbf{k}_{out}^{op} + \left(\frac{n_1}{n_2}\right)^2 \left[\mathbf{k}_{in} \cdot \mathbf{k}_{in} - (\mathbf{n} \cdot \mathbf{k}_{in})^2 \right]$$

Let $|\mathbf{k}_{in}| = |\mathbf{k}_{out}| = 1$, such that:

$$k_{out}^{op} = \sqrt{1 - \left(\frac{n_1}{n_2}\right)^2 \left[1 - (\mathbf{n} \cdot \mathbf{k}_{in})^2\right]}.$$

Using this result, we can fully express \mathbf{k}_{out} as a function of the surface normal vector \mathbf{n} and the incident light beam direction vector \mathbf{k}_{in} :

$$\mathbf{k}_{out}(\mathbf{n}, \mathbf{k}_{in}) = \left(\sqrt{1 - \left(\frac{n_1}{n_2}\right)^2 \left[1 - (\mathbf{n} \cdot \mathbf{k}_{in})^2\right]} - \left(\frac{n_1}{n_2}\right) (\mathbf{n} \cdot \mathbf{k}_{in}) \right) \cdot \mathbf{n} + \left(\frac{n_1}{n_2}\right) \mathbf{k}_{in}$$

This expression solely depends on scalar products enabling fast computation instead of lengthy trigonometric relations. During literature research, we found that this formula is/was used in efficient raytracing applications. We have created an interactive math3d.org project [13] to help the reader visualizing all the relationships. During literature research, we found that raytracing applications use this kind of formula, which is vastly unknown in spectroscopy. Further reading can be found in [11] [12] [9] [10].

Snell's law - example calculation

The arcing effect seen in our prism example in the main text only arises from an oblique incidence on an optical surface. We will now calculate a simple example of a light beam travelling in vacuum ($n_1 = 1$) parallel to the xz -plane at an angle ϕ relative to the z -axis (see Figure Figure 2a, *Prism Perspective* coordinate axis).

Let:

$$n_1 = 1, n_2 = 2 \quad \text{and} \quad \mathbf{n} = \frac{1}{\sqrt{2}} \begin{pmatrix} 0 \\ -1 \\ 1 \end{pmatrix}, \quad \mathbf{k}_{in} = \begin{pmatrix} \cos \phi \\ 0 \\ \sin \phi \end{pmatrix} \implies \mathbf{n} \cdot \mathbf{k}_{in} = \frac{1}{\sqrt{2}} \sin \phi.$$

Inserting this into the vectorial equation $\mathbf{k}_{out}(\mathbf{n}, \mathbf{k}_{in})$ gives:

$$\mathbf{k}_{out} = \left[\sqrt{1 - \left(\frac{1}{2}\right)^2 \left(1 - \left(\frac{1}{\sqrt{2}} \sin \phi\right)^2\right)} - \left(\frac{1}{2}\right) \left(\frac{1}{\sqrt{2}} \sin \phi\right) \right] \cdot \frac{1}{\sqrt{2}} \begin{pmatrix} 0 \\ -1 \\ 1 \end{pmatrix} + \left(\frac{1}{2}\right) \begin{pmatrix} \cos \phi \\ 0 \\ \sin \phi \end{pmatrix}. \quad (6)$$

Simplifying the equation further yields:

$$\mathbf{k}_{out} = \frac{1}{4} \left[\sqrt{6 + \sin^2 \phi} - \sin \phi \right] \begin{pmatrix} 0 \\ -1 \\ 1 \end{pmatrix} + \frac{1}{2} \begin{pmatrix} \cos \phi \\ 0 \\ \sin \phi \end{pmatrix}.$$

In our laboratory coordinate system (c.f. Figure 2a, *Prism Perspective*) the x -coordinate can be expressed as $x = \cos \phi$, thus, $\phi = \arccos x$. We can then write \mathbf{k}_{out} as a function of x . It is useful to calculate $\sin(\arccos x) = \sqrt{1 - x^2}$.

$$\mathbf{k}_{out} = \frac{1}{4} \left[\sqrt{7 - x^2} - \sqrt{1 - x^2} \right] \begin{pmatrix} 0 \\ -1 \\ 1 \end{pmatrix} + \frac{1}{2} \begin{pmatrix} x \\ 0 \\ \sqrt{1 - x^2} \end{pmatrix}$$

To investigate what curve \mathbf{k}_{out} is tracing out in the xy -plane, we can solely focus on the y -coordinate as a function of x .

$$Arc(x) = y(x) = -\frac{1}{4} \left(\sqrt{7 - x^2} - \sqrt{1 - x^2} \right).$$

The traced-out arc consists of the difference between two ellipses.

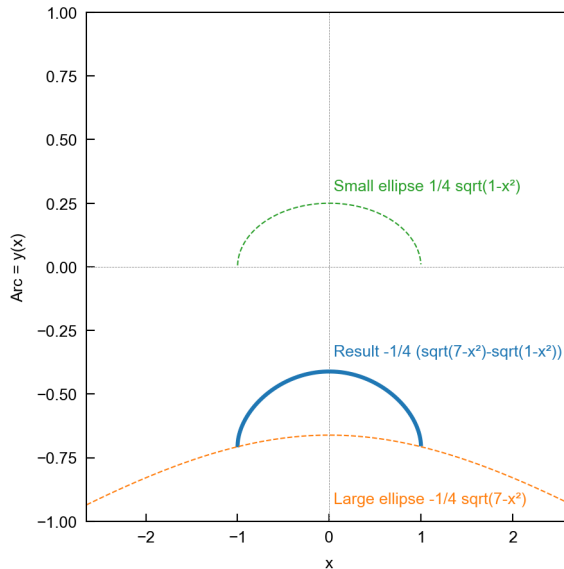


FIG. 6. Resulting arc (blue) that is the difference of a large ellipse (orange) and a small ellipse (green).

We plotted $Arc(x)$ (blue) in the figure above to give an example to the reader.

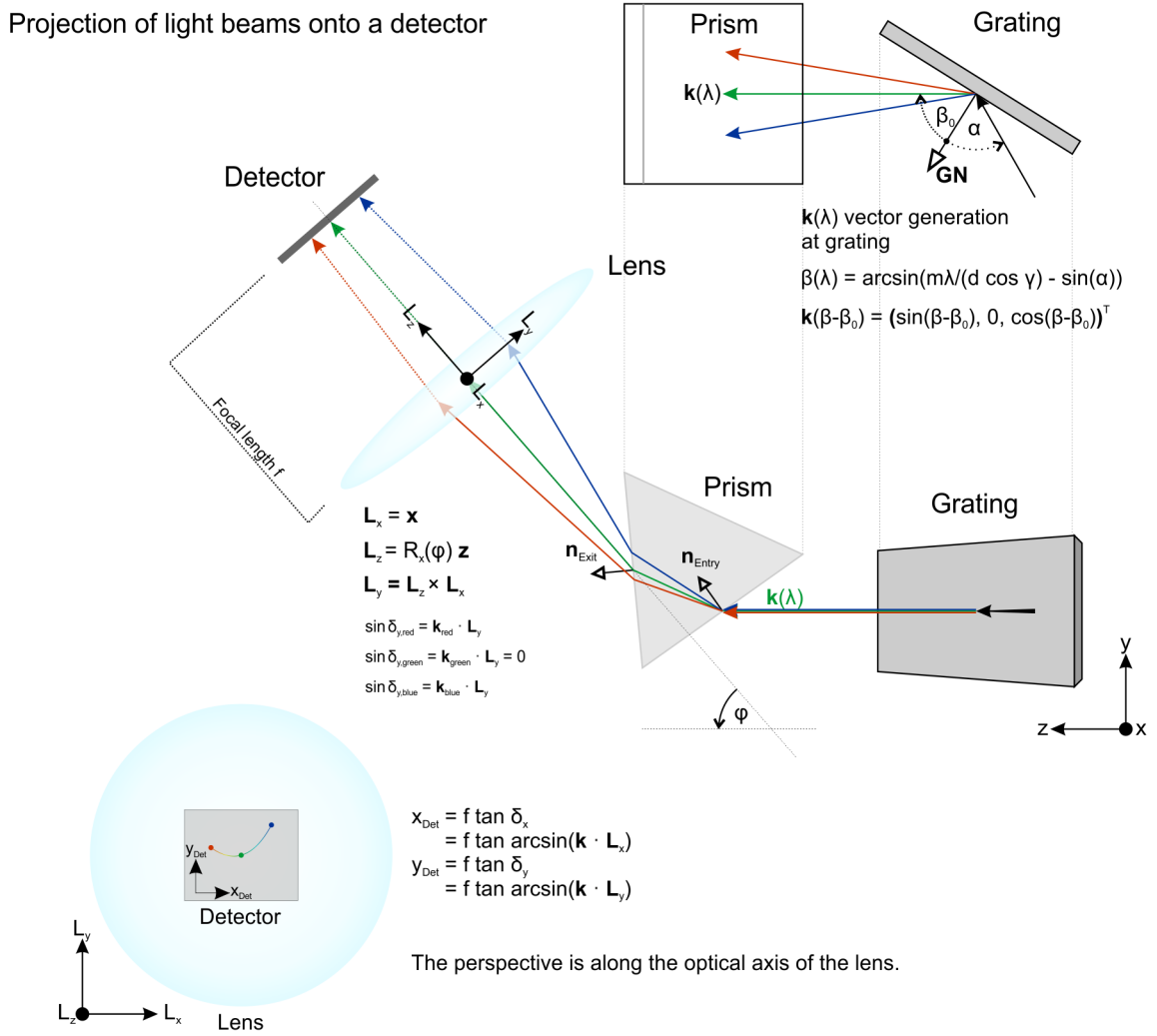


FIG. 7. Modelling approach of Échelle spectrometers.

Simulation principle and projections

We carry our simulations out mostly by using Python3 (<https://www.python.org>), with the packages astropy, numpy, scipy, and matplotlib. The procedure is as follows:

- Define a laboratory coordinate system $\{\mathbf{x}, \mathbf{y}, \mathbf{z}\}$
- Define the normal vectors of the prism $\{\mathbf{n}_{EntryFacet}, \mathbf{n}_{ExitFacet}\}$ in beam direction.
- Define a lens coordinate system $\{\mathbf{L}_x, \mathbf{L}_y, \mathbf{L}_z\}$ for the image generation and projections \mathbf{L}_z represents the optical axis. \mathbf{L}_x and \mathbf{L}_y help to project incoming beams within an orthogonal system. Example:
 - Rotate the \mathbf{z} unit vector around \mathbf{x} by ϕ via the rotation matrix $R_x(\phi)$ to generate \mathbf{L}_z
 - Define $\mathbf{L}_x = \mathbf{x}$
 - Calculate $\mathbf{L}_y = \mathbf{L}_z \times \mathbf{L}_x$
- Define a wavelength range array $\lambda[i]$ from 350 nm to 1150 nm
- Calculate an array of normalized \mathbf{k} vectors $\mathbf{k}_{in}[j]$ in the laboratory coordinate system $\{\mathbf{x}, \mathbf{y}, \mathbf{z}\}$ using the grating equation with an offset angle β_0 (see figure) and the array $\lambda[i]$ that will enter the next optical element. Here, the prism.

- For every \mathbf{k}_{in} vector, calculate the transmitted \mathbf{k}_{out} vector within the prism medium and repeat this for the light ray leaving the prism. Normalize the output vectors and compare for control. Snell's law may not change the length.
- Project the \mathbf{k} vector after the prism onto the Lens coordinate axes. The resulting angles are needed to deduce the position on the detector when using the Lens equation $(x, y) = f \tan(\delta_{(x,y)})$, where f is the focal length. The detector can be defined collinear to the Lens coordinate system. $\mathbf{x}_{Det} = \mathbf{L}_x$, $\mathbf{y}_{Det} = \mathbf{L}_y$. Yet, if needed, it is possible to rotate the lens coordinate system around an arbitrary vector (e.g. around the optical axis). SCIPY has very handy classes and methods to achieve this. Now the projected \mathbf{k} vectors will be rotated on the detector.

```

import numpy as np

@dataclass(init=True, repr=True)
class Ray:
    lambda: float
    color: str
    direction: np.ndarray

def refraction_on_surface(beam_vector, surface_normal, refractive_index_1, refractive_index_2):
    """
    Snell's law in vector form
    -----
    """
    vec_k = np.asarray(beam_vector)
    vec_sn = np.asarray(surface_normal)
    n1 = np.asarray(refractive_index_1, dtype=np.float64)
    n2 = np.asarray(refractive_index_2, dtype=np.float64)
    return (np.sqrt( 1 - ((n1/n2)**2) * (1 - np.dot(vec_sn, vec_k)**2) ) \
        - (n1/n2) * np.dot(vec_sn, vec_k)) * vec_sn + (n1/n2)*vec_k

def grating_b(m, l, d, a, g):
    """
    Return the outgoing angle of a light ray for a given order m with a given wavelength
    and incident angles
    """
    return np.arcsin( ((m * l)/(d * np.cos(g))) - np.sin(a) )

for m in np.arange(-minimum_visible_order, -maximum_visible_order, -1):
    x_list = []
    y_list = []
    ray_list = []

    for lambda in spectrum:
        angle = grating_b(m, lambda, d, grating_a, grating_g) - (grating_b0)
        ray = Ray(lambda, wavelength_to_rgb(lambda), np.asarray([np.sin(angle), 0, np.cos(angle)]))
        if (abs(angle) <= cam_fov_x_half):
            k_i = ray.direction
            k_in = k_i/np.linalg.norm(k_i)
            k_medium = \
                refraction_on_surface(k_in, prism_entry_surface_normal, n_air, sellmeier_n(ray.lambda))
            k_out = \
                refraction_on_surface(k_medium, prism_exit_surface_normal, sellmeier_n(ray.lambda), n_air)
            k_on = k_out/np.linalg.norm(k_out)

            # Project the resulting beam onto the optical axis of the lens
            # k_on • Lx = cos(..) → k_on • Lx = cos(90-a) → k_on • Lx = sin(a)
            a = np.arcsin(np.dot(k_on, Lx))
            g = np.arcsin(np.dot(k_on, Ly))
            x_pixel = x_pixels/2 + np rint( (1/px_size) * focal_length*np.tan(a))
            y_pixel = y_pixels/2 + np rint( (1/px_size) * focal_length*np.tan(-g))
            x_list.append(x_pixel)
            y_list.append(y_pixel)

```

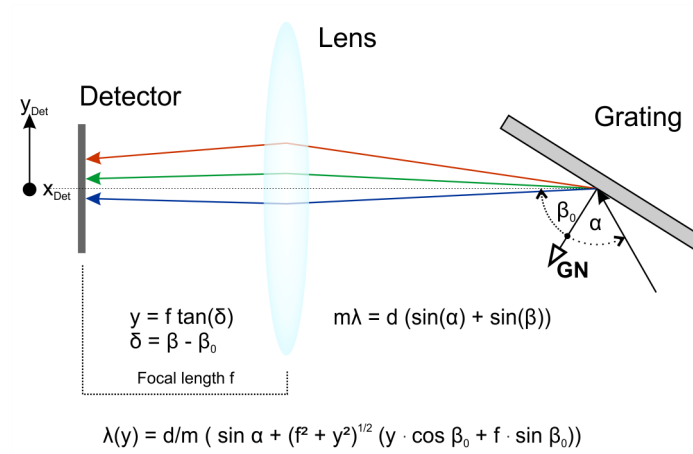


FIG. 8. General dispersion formula for a reflective diffraction grating and a lens positioned at an angle β_0 relative to the grating normal \mathbf{GN} .

Thoughts on grating dispersion and order calibration

Prisms as cross-dispersers untangle the overlapping grating orders and colours as shown in the main text in Figure 1. They have no influence on the initial grating dispersion that happens in the plane of incidence. Thus, we can simply treat the system as grating plus a lens. Here, we see a lens with its optical axis being at an angle β_0 relative to the grating normal vector \mathbf{GN} . By combining the grating and focusing equations, and using trigonometric identities, we obtain:

$$\lambda(y) = \frac{d \cdot \cos \gamma}{m} \left(\sin \alpha + \frac{1}{\sqrt{f^2 + y^2}} (y \cdot \cos \beta_0 + f \cdot \sin \beta_0) \right)$$

This equation can help to predict the in-plane position of spectral lines on a detector. Especially with negligible detector rotation. This is independent of any arcing from an oblique incidence on a prism.

Overlap between measurement and prediction

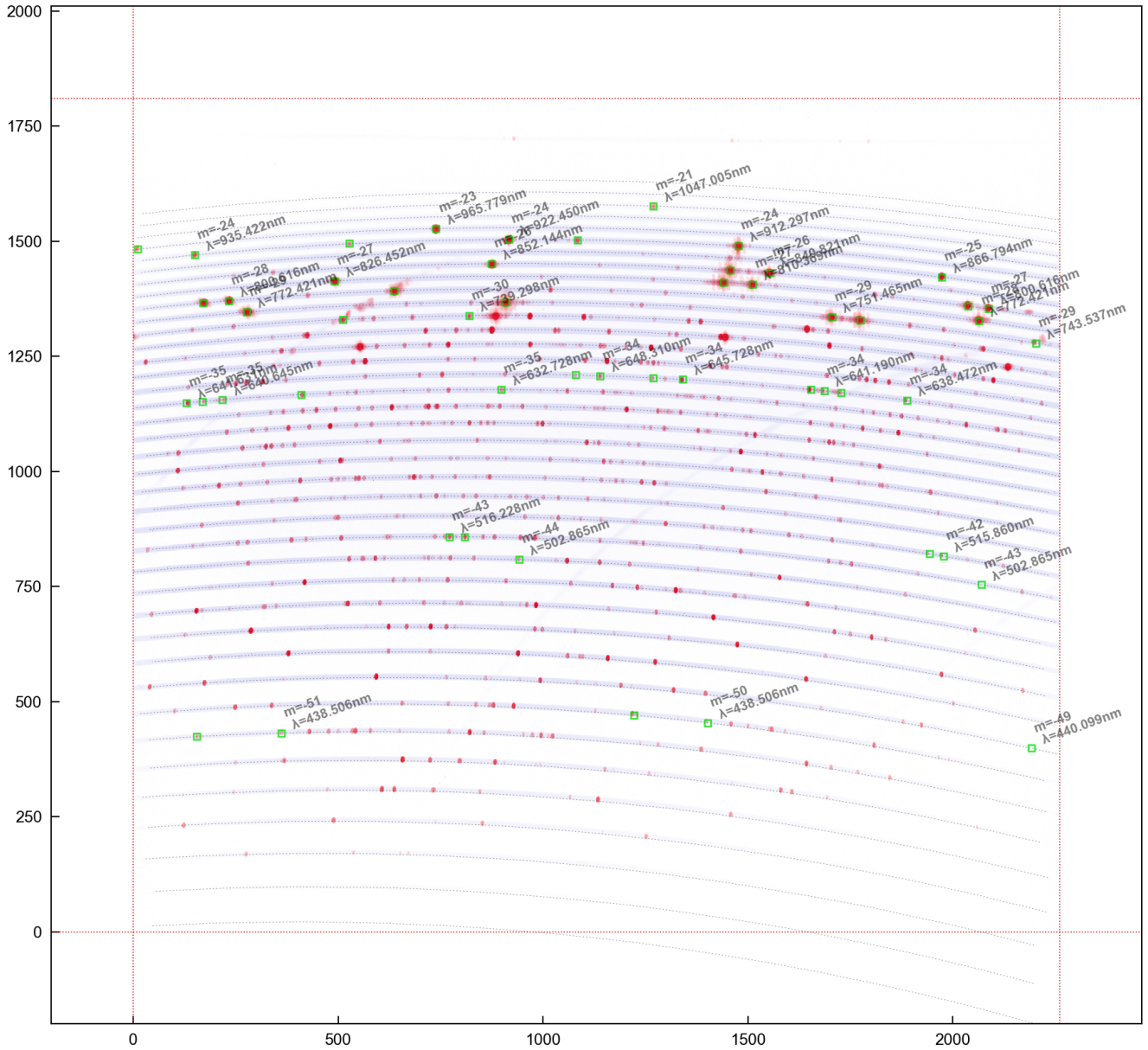


FIG. 9. General dispersion.

Figure 9 shows the overlap between a measured spectrogram (light blue, flat field image) and the predicted spectrogram (dotted, black). It is the magnified version Figure 3a. The red dots are measured ThAr peaks within the visible orders. The green boxes denote simulated positions of randomly selected Ar and Th lines from NIST [16]. The absolute orders and wavelengths in nanometres are added to every other green box for clarity. It is evident, that the predicted and measured orders nicely overlap, showing that the algorithm works dependably. For this to work ad-hoc one needs to understand the geometry of the spectrograph (incident angles) as well as the focal length of the objective in front of the detector. Note: This spectrogram was taken on a home-built FLECHAS spectrograph by Bernd Bitnar. The built-up was supported by Karl-Heinz Wolf and Klaus Vollmann.

FLECHAS spectrometer

The FLECHAS spectrometer created by the CAOS group (<https://spectroscopy.wordpress.com/2017/06/22/flechas-opto-mechanical-components/>) is a f/18 spectrometer with a resolution of $\delta\lambda/\lambda$ of 7000 – 11000 without an image slicer. The parabolic mirror has a focal length of $f = 444$ mm resulting in a beam diameter of 25 mm. Please refer to their excellent homepage containing years of experience and several spectrometers built by CAOS [14].